

# The role of PET quantification in cardiovascular imaging

Piotr Slomka · Daniel S. Berman · Erick Alexanderson ·  
Guido Germano

Received: 10 March 2014 / Accepted: 7 July 2014 / Published online: 1 August 2014  
© Italian Association of Nuclear Medicine and Molecular Imaging 2014

**Abstract** Positron emission tomography (PET) has several clinical applications in cardiovascular imaging. Myocardial perfusion imaging with PET allows accurate global and regional measurements of myocardial perfusion, myocardial blood flow and function at stress and rest in a single examination. Simultaneous assessment of function and perfusion by PET with quantitative software is currently routine practice. Combination of ejection fraction reserve with perfusion information may improve the identification of severe coronary artery disease. Myocardial viability can be estimated by quantitative comparison of fluorine-18 fluorodeoxyglucose ( $^{18}\text{F}$ -FDG) and rest perfusion imaging. Quantitative myocardial blood flow and myocardial flow reserve measurements are becoming routinely included in clinical assessments due to the enhanced dynamic imaging capabilities of the latest PET/CT scanners. Absolute flow measurements allow evaluation of

coronary microvascular dysfunction and provide additional prognostic and diagnostic information in coronary disease. Quantitative clinical software tools for computing myocardial blood flow from kinetic PET data in an automated and rapid fashion have been developed for use with several radiotracers:  $^{13}\text{N}$ -ammonia,  $^{15}\text{O}$ -water and  $^{82}\text{Rb}$ . The level of agreement between various software methods available for such analyses is excellent. Relative quantification of  $^{82}\text{Rb}$  PET myocardial perfusion tracer uptake, based on comparisons with normal perfusion databases, demonstrates high performance for the detection of obstructive coronary disease. Computerized analysis of myocardial perfusion at stress and rest reduces the variability of the assessment compared with visual analysis. New tracers, such as  $^{18}\text{F}$ -flurpiridaz may allow further improvements in myocardial blood flow quantification and disease detection. PET quantification can be enhanced by precise coregistration with CT angiography. In emerging clinical applications, the potential to identify vulnerable plaques by quantification of atherosclerotic plaque uptake of  $^{18}\text{F}$ FDG and  $^{18}\text{F}$ -sodium fluoride tracers in carotids, aorta and coronary arteries has been demonstrated.

Color figures online at <http://link.springer.com/article/10.1007/s40336-014-0070-2>.

P. Slomka (✉) · D. S. Berman · G. Germano  
Department of Imaging and Medicine, Cedars-Sinai Heart  
Institute, Cedars-Sinai Medical Center, Los Angeles, CA, USA  
e-mail: piotr.slomka@cshs.org

P. Slomka · G. Germano  
David Geffen School of Medicine, University of California Los  
Angeles, Los Angeles, CA, USA

E. Alexanderson  
Cardiovascular Imaging and Nuclear Cardiology Department,  
Instituto Nacional de Cardiología ‘Ignacio Chávez’, Mexico,  
Mexico

E. Alexanderson  
Facultad de Medicina, Universidad Nacional Autónoma de  
México, Mexico, Mexico

**Keywords** PET · Quantification · Cardiovascular  
imaging · Myocardial perfusion imaging · Flow reserve ·  
Ejection fraction

## Introduction

Positron emission tomography (PET) allows accurate measurement of relative myocardial hypoperfusion, absolute myocardial blood flow and contractile function at stress and rest, in a single scanning session, allowing diagnosis of coronary artery disease (CAD) [1] and

evaluation of long-term prognosis [2]. PET is considered the gold standard for measuring myocardial blood flow [3, 4] and it is also an important tool in assessment of the viability of the myocardium [5]. New cardiac PET imaging techniques are being developed to investigate plaque inflammation in the cardiovascular system [6]. The multitude of information that can be obtained from PET images necessitates the use of advanced quantitative techniques. Some parameters, such as absolute myocardial blood flow measurements, cannot be obtained by visual analysis alone. In addition, quantitative or semi-quantitative analysis of PET data, compared with visual interpretation, allows reduced inter- and intra-observer variability.

Software quantification methods for cardiac PET have evolved recently, and they allow rapid and largely automated extraction of various physiological parameters. Typically, a PET quantification software package allows integrated analysis of static, gated and dynamic datasets in a single session, facilitating inclusion of all quantification results in the clinical review. These various image datasets can be obtained from a single PET acquisition of the list-mode data—this is typically possible with the latest scanners. Static images are used to define the extent and severity of regional hypoperfusion at stress and rest. Viability imaging performed with a glucose analog—fluorine-18 fludeoxyglucose ( $^{18}\text{F}$ -FDG)—makes it possible to define the amount of myocardial scar (no uptake of  $^{18}\text{F}$ -FDG or perfusion tracer) and mismatch (uptake of  $^{18}\text{F}$ -FDG but no myocardial perfusion uptake). Gated PET images allow automated computation of left ventricular volumes, ejection fraction (EF) and other functional parameters, such as diastolic function. Finally, dynamic reconstruction of the data allows extraction of the time-activity curves from the blood pool and myocardium, and computation of absolute regional myocardial blood flow in ml/g/min at stress and rest and consequently myocardial flow reserve (MFR)—defined as the ratio of myocardial blood flow at stress and rest. These computations can be obtained within seconds, with minimal user interaction.

This review describes state-of-the-art PET quantification techniques, focusing particularly on applications currently in clinical use and summarizing their role in cardiovascular disease detection and management.

### Relative quantification of perfusion and ischemia

Positron emission tomography myocardial perfusion is recommended for diagnosis or risk stratification of patients who have non-diagnostic results on other imaging tests [7]. Cardiac PET/CT, through analysis of perfusion changes between stress and rest (ischemia) and comparison of perfusion studies with normal limits derived from images

of subjects with low likelihood of disease and normal perfusion findings, allows detection of obstructive CAD [8–10]. The relative quantification technique based on normal limits is widely used in single-photon emission computed tomography (SPECT) and has been adapted to PET imaging. Typically, an integrated score combining hypoperfusion severity and extent is derived using the polar map concept. Quantitative analysis of relative hypoperfusion has been shown to rival the accuracy of expert readers in the diagnosis of CAD by SPECT in large studies [11]. The key advantage of such quantitative analysis is its improved reproducibility compared with visual assessment [12].

In previous reports of cardiac PET diagnostic performance for CAD detection, the average sensitivity for detecting at least one coronary artery with significant stenosis was 89 % (range 83–100 %), and the average specificity was 89 % (range 73–100 %) [13], even though it is accepted that there is no 1-to-1 relationship between obstructive disease and ischemic stenosis [14]. Most of the early PET perfusion studies were obtained with stand-alone 2D PET scanners rather than with integrated PET/CT systems and utilized visual scoring of perfusion defects in a 17-segment model, which is analogous to SPECT perfusion scoring. Although automated relative quantification was initially developed for SPECT imaging, several recent studies report the use and performance of this method in PET/CT imaging. To date, three studies have reported  $^{82}\text{Rb}$  PET/CT diagnostic performance with quantitative analysis based on comparison with normal limits (Fig. 1) [9, 10, 15]. Kaster et al. [15] achieved perfect 100 % sensitivity for the detection of obstructive CAD when transient ischemic dilation results were integrated with perfusion results. Figure 2 shows examples of perfusion images and quantification results based on normal limits and the direct stress-rest comparison for  $^{82}\text{Rb}$ . Although separate normal limits are typically required for males and females in SPECT quantification, relative PET perfusion quantification methods use combined-gender normal limits; this is possible owing to the accurate CT attenuation correction available on PET/CT scanners [9, 10, 15]. It should be noted that due to variable characteristics of normal perfusion distribution for different tracers, for example reduced isotope concentration in the lateral wall on  $^{13}\text{N}$ -ammonia imaging [16], relative analysis of PET perfusion will require isotope-specific normal limits.

### Quantification of heart contractile function

The quantitative analysis of myocardial contractile function has been extensively validated for myocardial SPECT [17], but such quantitative methods can be also applied to PET. A

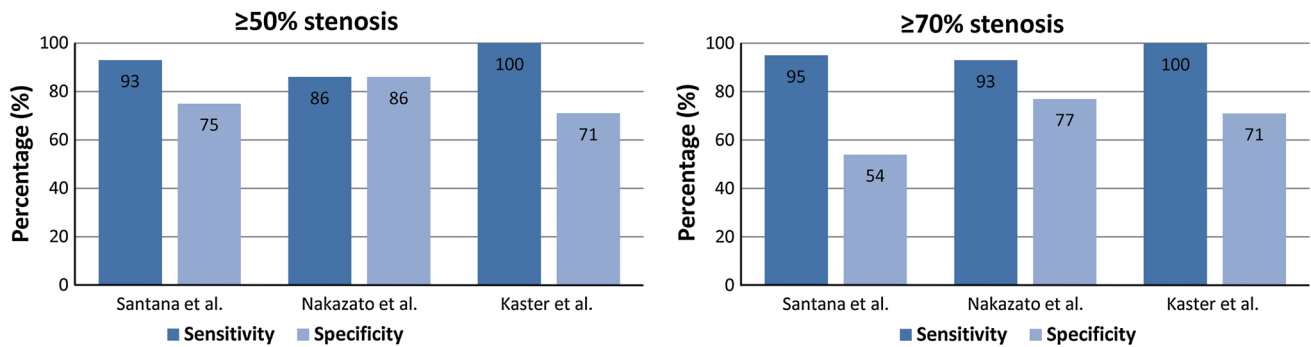
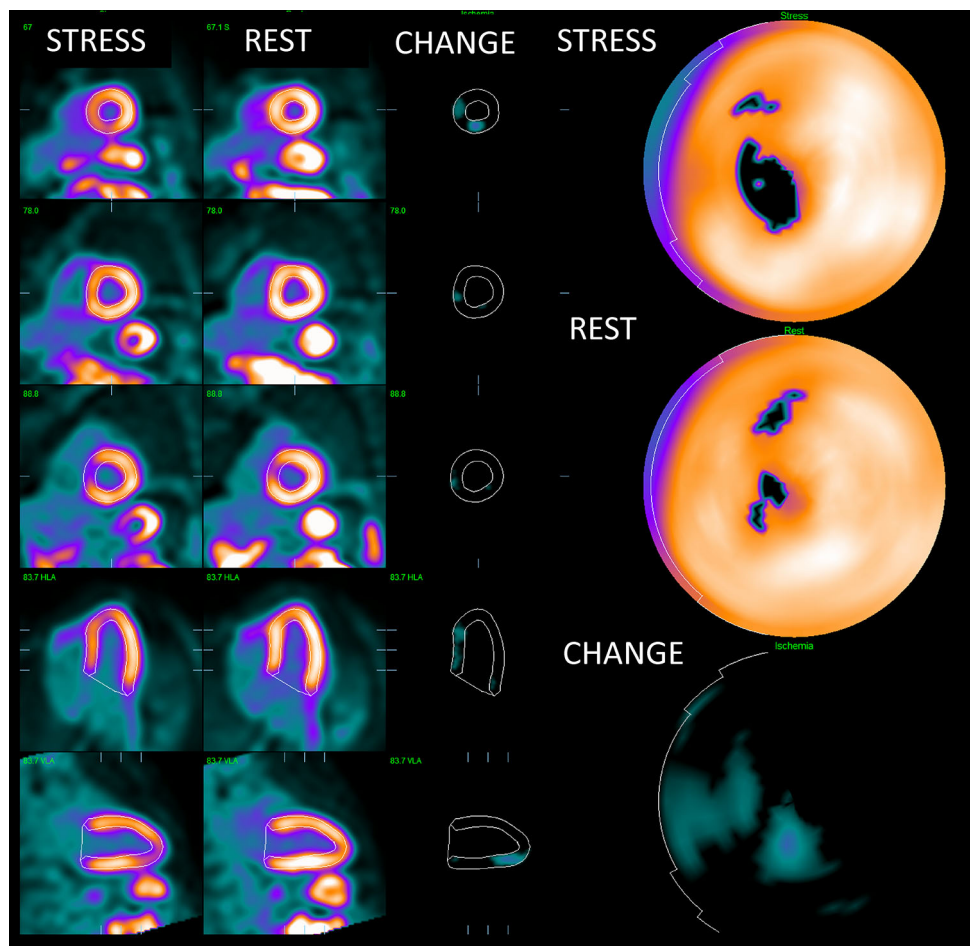


**Fig. 1** Relative quantification accuracy. Results from three recent manuscripts by Santana et al. [9] ( $n = 76$ ), Nakazato et al. [10] ( $n = 167$ ), and Kaster et al. [15] ( $n = 110$ ), validating the use of

relative quantification with normal limits in myocardial perfusion PET studies for detection of coronary artery disease by three separate software tools (color figure online)

**Fig. 2** An example of relative quantification for myocardial perfusion PET. Co-registered stress and rest images with contours are shown on the left. The change images (CHANGE) in the middle show the ischemic region in the septal wall. Polar maps (right) show corresponding significant defect at stress. The quantification results were stress total perfusion deficit (TPD) = 10 %, rest TPD = 4 %, ischemia by change analysis = 5 %. Ejection fraction was normal. This patient had significant >70 % lesion in the proximal left anterior descending territory as confirmed by angiographic examination (color figure online)



typical contemporary protocol for PET imaging includes list-mode data acquisition at stress and rest. This allows retrospective reformatting and re-binning with cardiac gating and subsequently derivation of gated data. An excellent correlation of MRI and PET  $^{18}\text{F}$ -FDG imaging techniques for quantification of EF as well as systolic and diastolic volumes has been reported [18, 19]. Compared with SPECT images, PET images exhibit higher resolution and better definition of

the mitral valve plane due to accurate attenuation correction [10]. This allows more accurate detection of the myocardium and improved tracking of the mitral valve plane. High PET image resolution and  $^{18}\text{F}$ -FDG uptake in the right ventricle may also allow quantification of right ventricular function by PET [20].

PET contractile function analysis can be used in conjunction with perfusion analysis to improve patient

risk stratification. In a study including 1441 patients, stress EF measured from  $^{82}\text{Rb}$  PET provided an independent and incremental prognostic value compared with perfusion measures [21]. Functional measurements from PET may also include phase and dyssynchrony analysis. Although these techniques have not been extensively validated with PET, measurements of histogram bandwidth and phase standard deviation from  $^{15}\text{O}$ -water and  $^{18}\text{F}$ -FDG-PET scans were found to be very well correlated with SPECT [22]. Recently, in an analysis of 486 patients, left ventricular mechanical dyssynchrony was found to be an independent predictor of all-cause mortality in ischemic cardiomyopathy [23]. Furthermore, an analysis of dyssynchrony obtained from gated  $^{18}\text{F}$ -FDG-PET imaging was shown to identify responders to cardiac resynchronization therapy [24]. Another quantitative parameter related to contractile function, first described and validated for SPECT, is the transient ischemic dilation of the left ventricle. This measure has been found to improve the identification of patients with severe CAD by SPECT [25]. Rischpler et al. [26] demonstrated the use of the transient ischemic dilation ratio in  $^{82}\text{Rb}$  PET imaging as an independent predictor of mortality.

A key advantage of PET perfusion imaging over SPECT perfusion imaging (wherein images are typically acquired at least 15 min after injection) is the possibility of performing immediate imaging of heart contractile function during stress. Thus, with PET imaging, it is possible to assess the true peak stress function. In contrast, with SPECT, given that scans are typically performed 15–45 min after stress, only post-ischemic changes due to myocardial stunning can be observed. Therefore, PET imaging allows quantification of the EF reserve—defined as the change in EF between stress and rest. In 510 patients, Dorbala et al. [27] showed that the EF reserve obtained with  $^{82}\text{Rb}$  PET imaging was the only independent predictor of left main and triple-vessel disease. A very high negative predictive value (97 %) for excluding severe left main and triple-vessel disease was demonstrated if the EF reserve was higher than 5 %. The same group has also shown that left ventricular EF reserve has incremental prognostic value over clinical variables and resting EF obtained from  $^{82}\text{Rb}$  PET [28]. Recently, the use of EF reserve quantification was evaluated for the regadenoson stress agent and  $^{82}\text{Rb}$  PET imaging. The mean left ventricular EF reserve was shown to be significantly higher in patients with normal myocardial perfusion imaging results ( $6.5 \pm 5.4$  %) than in those with mild ( $4.3 \pm 5.1$  %,  $p = 0.03$ ) and moderate-to-severe reversible defects ( $-0.2 \pm 8.4$  %,  $p = 0.001$ ). Also, the mean left ventricular EF reserve was significantly higher in patients with a low likelihood of CAD ( $7.2 \pm 4.5$  %,  $p < 0.0001$ ) [29].

### Myocardial blood flow and myocardial flow reserve quantification

Myocardial blood flow and MFR measurements are becoming routinely included in clinical assessments due to the enhanced dynamic imaging capabilities of the latest PET/CT scanners. PET allows non-invasive measurements in units of milliliters of blood per minute, per gram of myocardium. These absolute measurements have been validated against invasive flow estimates obtained by microsphere techniques in numerous studies. PET is currently the most validated imaging technique for the quantitative evaluation of myocardial blood flow.

New software tools are now becoming available that will allow more widespread quantification of myocardial blood flow at stress and rest. These tools include kinetic models and algorithms for computing myocardial blood flow and MFR from kinetic PET data obtained using different radiotracers:  $^{13}\text{N}$  ammonia [30, 31],  $^{15}\text{O}$ -water [32] and  $^{82}\text{Rb}$  [33]. Current software tools utilizing these algorithms allow completely automated or semi-automated measurements of stress and rest flow. Figure 3 shows screenshots of the three implementations of recent clinical software for computation of myocardial blood flow and MFR. The input function is typically obtained from the first-pass blood pool analysis in the left ventricle or left atrium. Segmentation of the left ventricle and determination of the blood pool region can be accomplished automatically. Patient motion correction can also be applied to improve the robustness of the analysis. The computations are rapid, typically being accomplished within seconds. Both global and regional (or segmental) myocardial blood flow and MFR measurements are obtained, by kinetic modeling techniques, assuming the appropriate compartmental model, which is specific to a given radiotracer. The inter-scan reproducibility of software methods for absolute flow measurements has been reported to be in the order of 15 % [34]. The quantitative agreement between different software methods available for such analyses is also very good, as recently evaluated for  $^{82}\text{Rb}$  [35] and  $^{13}\text{N}$ -ammonia [36] models (Fig. 4). Clinically,  $^{82}\text{Rb}$  PET blood flow measurements have the widest application, since  $^{82}\text{Rb}$  does not require a cyclotron on site. Although the  $^{82}\text{Rb}$  is not a tracer with ideal imaging properties—for example it has a lower extraction fraction than other tracers—the  $^{82}\text{Rb}$  flow measurements have been well validated and calibrated to both  $^{13}\text{N}$ -ammonia [33] and  $^{15}\text{O}$ -water [37] measurements.

Absolute flow measurements and MFR estimation allow evaluation of several clinically important cardiovascular conditions. Flow measurements at stress and rest provide an integrated measure of the ischemic burden due to microvascular and macrovascular disease [38]. Myocardial flow measurements at stress may potentially allow identification

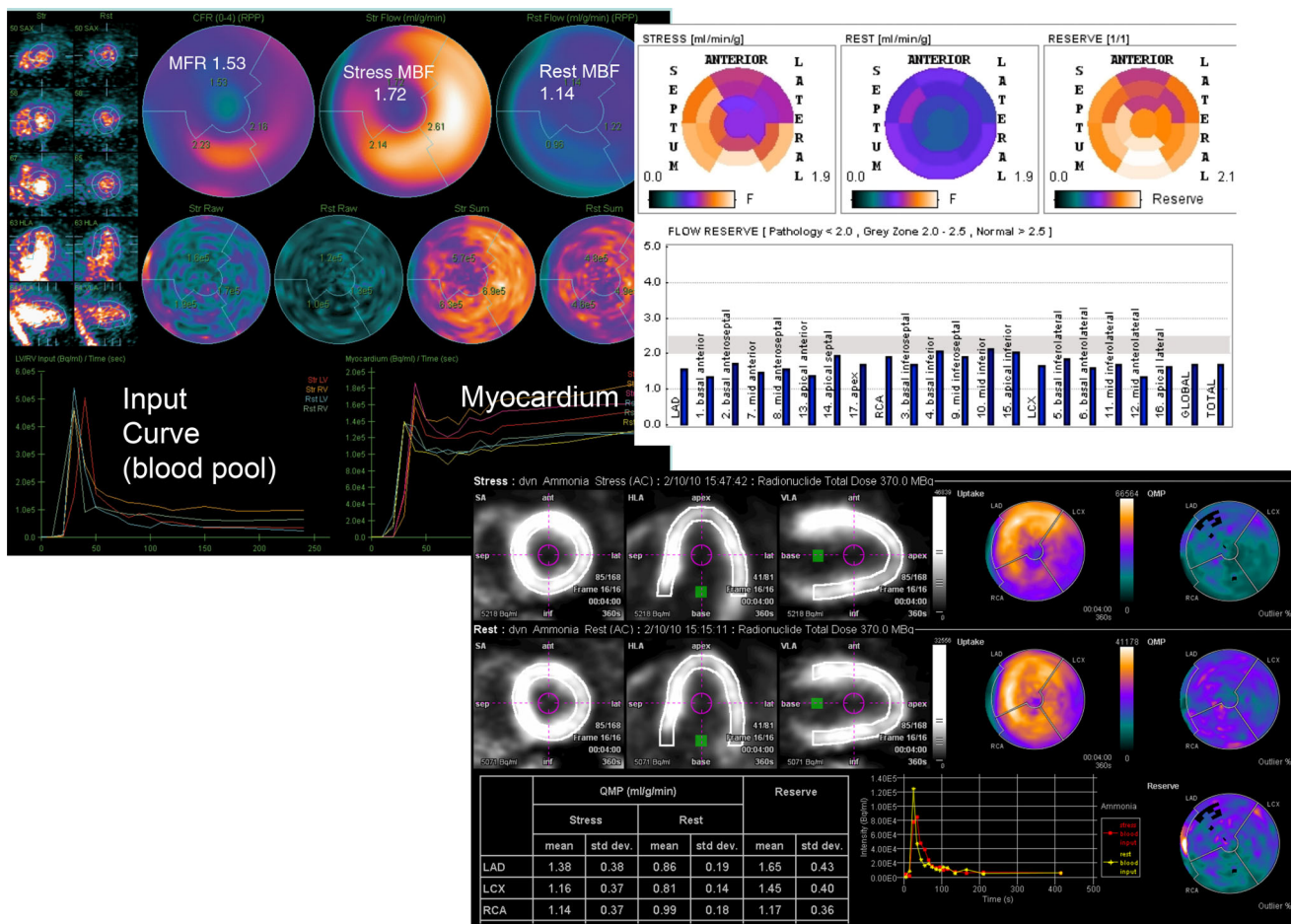


**Fig. 3** Results from different implementations of the absolute flow quantification methods demonstrating regional and segmental quantification of rest and stress myocardial blood flow and myocardial

flow reserve. Cedars Sinai QPET (top left) PMOD software (top right) and Siemens syngoMBF flow analysis (bottom) are shown (color figure online)

of endothelial dysfunction in early coronary disease [38]. In addition, resting myocardial flow heterogeneity and in particular gradient of flow reduction from the base to the apex of the left ventricle has been demonstrated to be a potential early marker of sub-clinical CAD [39]. The presence of a normal MFR can also confirm adequate pharmacological response in the absence of disease [40]. On the other hand, an MFR value <1 could be a hallmark of coronary steal, which is a dangerous clinical condition [41, 42]. Therefore, these quantitative measurements provide powerful additional prognostic and diagnostic information, which could be utilized clinically. Figure 5 shows an example of severely reduced MFR in all the territories observed in microvascular disease. Relative quantification shows only a small abnormality in this case. Patients in whom this condition is diagnosed by quantification of MFR could benefit from aggressive lipid-lowering therapy [43].

Currently, diagnoses of significant, obstructive CAD by PET are typically achieved by visual or quantitative assessment of the relative hypoperfusion at stress and rest rather than

by absolute flow quantification. Nevertheless, myocardial flow measurements have also been shown to be useful in the diagnosis of CAD, especially in the detection of multivessel CAD. It has been reported that quantification of <sup>82</sup>Rb net retention, to measure the stress-rest blood flow difference in the myocardium, defined a greater extent of disease than did standard quantification based on comparisons of the relative stress-rest perfusion difference [44]. Ziadi et al. [45] studied the incremental value of absolute MFR over standard relative quantification in 120 patients undergoing rest/stress <sup>82</sup>Rb imaging. They found that the MFR defined by PET was an independent predictor of triple-vessel CAD and provided added value to relative quantification by summed stress scoring. In a related study by Fiechter et al. [46], absolute measurements of MFR were found to increase the per-patient diagnostic accuracy of <sup>13</sup>N-ammonia from 79 to 92 % in 73 patients. Figure 6 shows an example of a PET <sup>82</sup>Rb scan with angiographically confirmed triple-vessel disease in which only two territories are identified as abnormal by relative quantification. These preliminary studies reporting increased

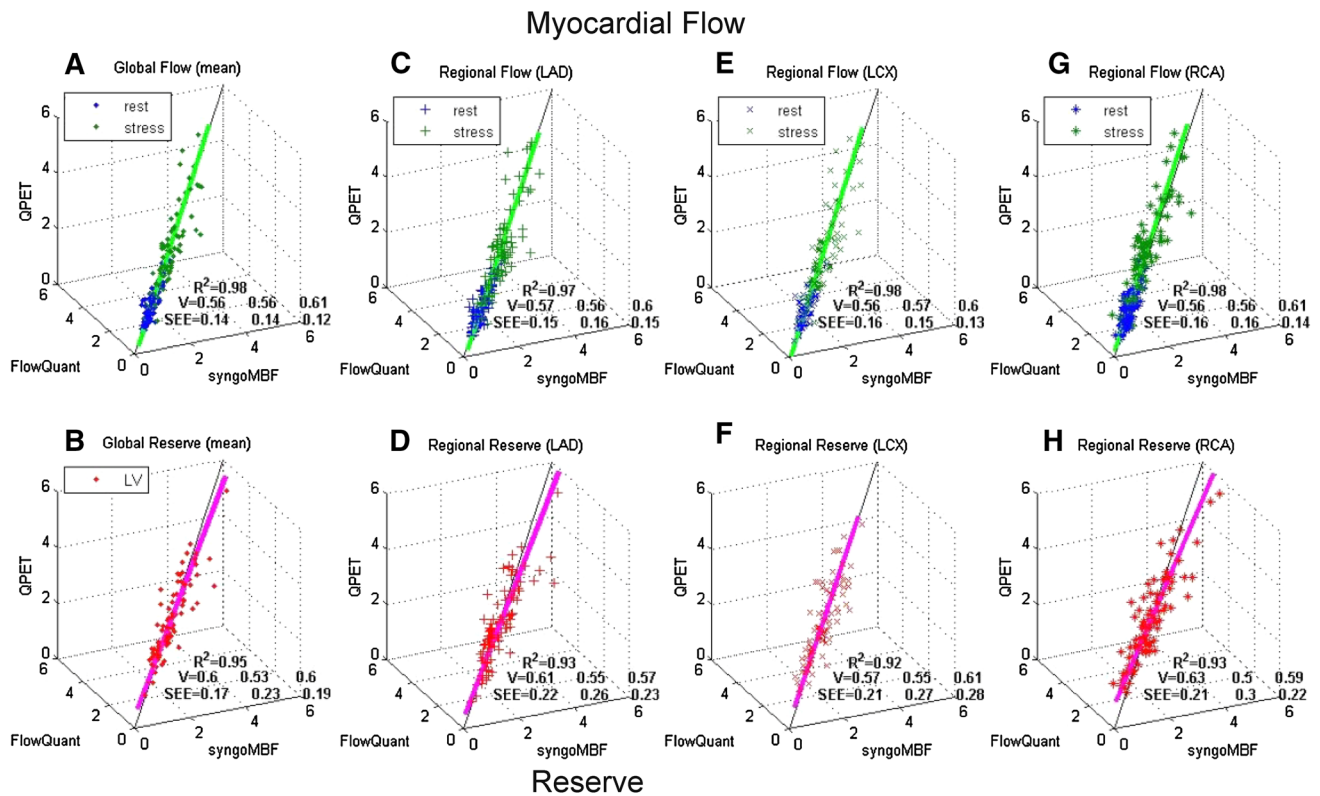


**Fig. 4** Agreement for the software packages on measurements of myocardial blood flow and myocardial flow reserve. 3D scatterplots of syngoMBF vs FlowQuant vs QPET values of rest and stress myocardial blood flow and myocardial flow reserve for global left ventricle (a, b) and regional vascular territories (c–h).  $R^2$  is the total

variance described by 3D unit basis vector (V) line of best fit. SEE is the standard deviation of residual errors from regression line of best fit for each of the three programs. Reproduced with permission from deKemp et al. [35] (color figure online)

diagnostic accuracy for detection of coronary disease with absolute flow measurements when combined with relative quantification will need to be confirmed in larger cohorts, since reduced absolute MFR measurements could be caused by factors other than CAD, or could be related to non-obstructive disease [38], thus reducing the specificity for the detection of the obstructive disease.

Quantification of MFR by PET has also recently been established as an important prognostic tool. MFR was shown to improve patient risk assessment compared with relative perfusion (summed stress scoring), and EF quantification alone [2]. Murthy et al., in a study of 2,782 patients, showed that the incorporation of MFR into cardiac death risk assessment resulted in correct reclassification of almost 35 % of intermediate-risk patients and a significant increase in c-index (from 0.82 to 0.84). Figure 7 shows the incremental prognostic value of MFR over ischemia measures. Based on this evidence, quantitative absolute myocardial flow measurements can be used to improve patient mortality risk stratification in addition to other PET measures, such as relative perfusion abnormality or EF.

The practicality of the routine clinical imaging with PET is challenged by the need for an on-site cyclotron (in the

case of  $^{13}\text{N}$ -ammonia and  $^{15}\text{O}$ -water imaging), or an on-site generator (in the case of  $^{82}\text{Rb}$  imaging). In addition,  $^{82}\text{Rb}$  does not have optimal imaging characteristics, due to its long positron range and low extraction fraction. A new imaging tracer,  $^{18}\text{F}$ -flurpiridaz, has recently been proposed for cardiac PET imaging [47]. This tracer exhibits high image contrast in the myocardium, and prolonged retention and superior extraction compared with SPECT tracers (Tc-99m or TI-201) or  $^{82}\text{Rb}$  PET. Cardiac PET imaging with  $^{18}\text{F}$ -flurpiridaz could be performed without a cyclotron on site, because of the relatively long half-life of this tracer. Although the longer half-life of  $^{18}\text{F}$ -flurpiridaz may result in higher patient doses compared with doses for  $^{82}\text{Rb}$  or  $^{13}\text{N}$ -ammonia PET, the reported doses are nevertheless less than 6.4 mSv for the full rest/stress study [48]. New myocardial blood flow quantification models have been proposed and validated for  $^{18}\text{F}$ -flurpiridaz. Sherif et al. [49] showed that the superior imaging characteristics of this tracer enable estimation of absolute flow values by simplified analysis of retention and standardized uptake values (SUVs). These properties of  $^{18}\text{F}$ -flurpiridaz open up new opportunities in the use of absolute quantification since SUV computations do not require the measurement of the

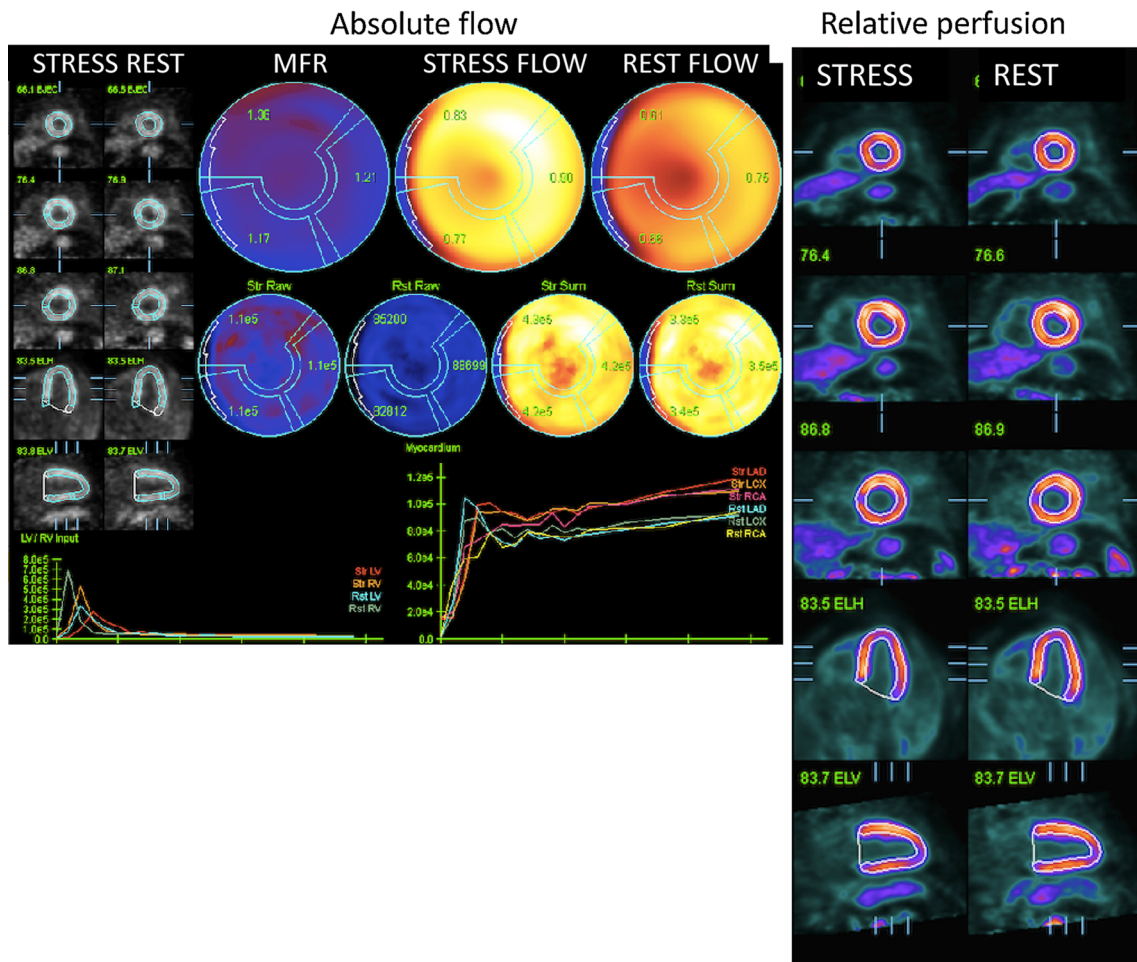


**Fig. 5** Example of severely reduced myocardial flow reserve (1.17–1.37) and reduced myocardial stress flow (0.83–0.77 ml/g/min) in all vascular territories in a patient with syndrome X (left).

This patient had a borderline abnormal relative perfusion scan with mildly decreased uptake at stress in the part of the inferior wall (right) (color figure online)

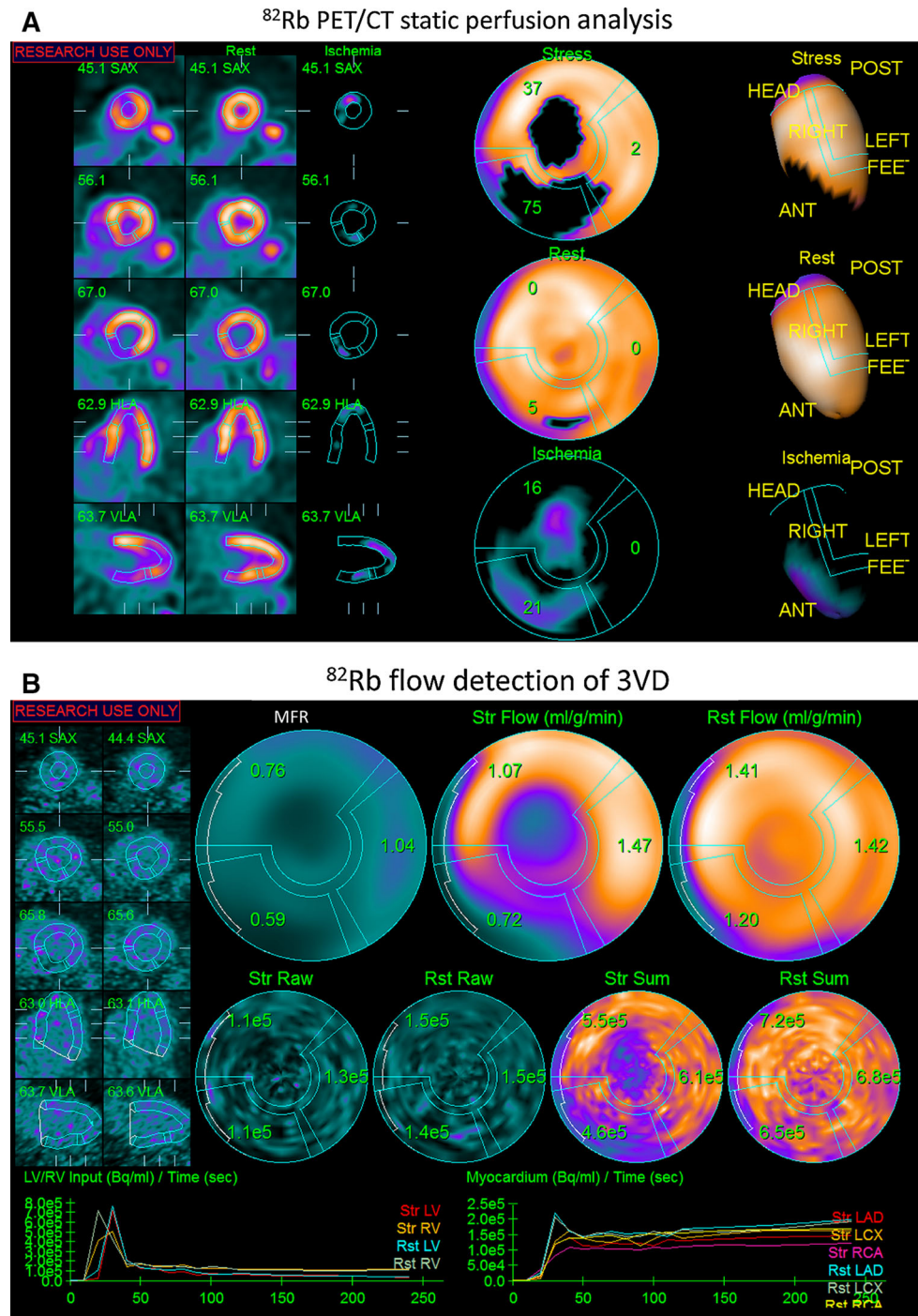
myocardial input function and thus would allow a treadmill exercise regimen outside of the scanner. Such simplified techniques may lead to a wider acceptance of the quantitative models. Furthermore, the high resolution of <sup>18</sup>F-flurpiridaz images may allow improved quantitative accuracy and may warrant the use of sophisticated techniques eliminating cardiac [50] and patient motion [51] to provide optimal quantitative results. In initial validation of <sup>18</sup>F-flurpiridaz, its diagnostic accuracy was reported to be higher than that of SPECT with visual scoring of static images in a phase II trial [48]; however, clinical application of this tracer for myocardial blood flow quantification has not yet been reported.

**Relative quantification of myocardial viability**

Positron emission tomography has been considered the most sensitive method and the “gold standard” for assessment of

myocardial viability [5, 52, 53]. In a simple static protocol, which has been accepted clinically, relative uptake of <sup>18</sup>F-FDG is measured and compared with perfusion at rest. PET viability imaging is used to identify patients with a significant amount of viable recoverable myocardium and can predict functional recovery [54]. The amount of viable myocardium has long-term prognostic implications [55–58]. Patients with viable myocardium will be more likely to benefit from revascularization than those who do not show such viable tissue. Typically, <sup>18</sup>F-FDG viability imaging is combined with a resting PET perfusion scan (using <sup>82</sup>Rb or <sup>13</sup>N-ammonia tracer) or even a resting SPECT scan. Regions which are hypoperfused at rest but are viable (have some <sup>18</sup>F-FDG uptake) are defined by combined assessment of both scans. If a certain degree of such mismatch between perfusion and viability is detected, it indicates that the patient may benefit from a revascularization procedure. Currently the usual clinical method for detecting such viability patterns is visual assessment of the mismatch between static images of

**Fig. 6** Example of added value of myocardial flow reserve (MFR) over ischemia quantification for diagnosis from  $^{82}\text{Rb}$  PET. Relative quantification of total perfusion deficit at stress and rest shows stress and ischemic abnormalities in left anterior descending and left circumflex territories but normal right coronary artery territory (a), while MFR is definitely abnormal in all vascular territories (0.76–1.04), with no flow reserve (MFR = 1.04) in the right coronary region (b). This case was angiographically confirmed as triple vessel disease (color figure online)



the resting perfusion defect and the static  $^{18}\text{F}$ -FDG-PET scan. However, visual methods for the identification of mismatch suffer from the usual problems of inter- and intra-observer variability. If a specific threshold is required for the decision on the intervention, automated quantitative techniques should be considered to ensure objective patient management. To this end, several relative quantification techniques which automatically compute the amount of mismatch and scar have been developed [17, 57, 59, 60].

In the first report on quantitative viability analysis, Beanlands et al. [59] proposed mismatch and scar scores derived from combined perfusion and viability polar maps. These parameters combine extent and severity of the defects. The Cedars-Sinai group has developed an integrated analysis of perfusion and viability in their software. Viability quantification is accomplished as follows: 3D left ventricular contours derived from resting PET or SPECT scans and  $^{18}\text{F}$ -FDG-PET images are co-registered in 3D to



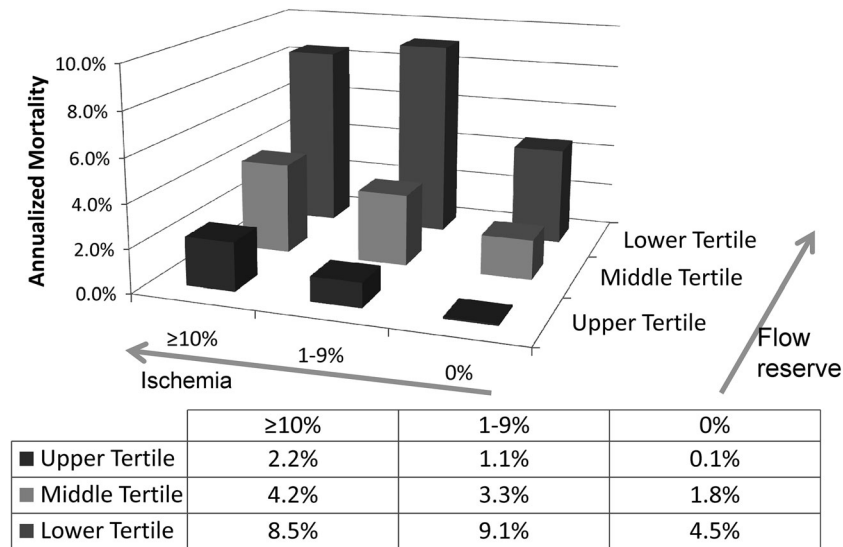


**Fig. 7** Incremental prognostic value of myocardial flow reserve (MFR) over ischemia measures. Unadjusted annualized cardiac mortality by tertiles of MFR and by categories of myocardial ischemia. The annual rate of cardiac death increased with increasing summed stress score and decreasing MFR. Importantly, lower MFR

consistently identified higher-risk patients at every level of myocardial scar/ischemia, also among those with visually normal positron emission tomography scans and normal left ventricular function. Reproduced with permission from Murthy et al. [2]

correct for rotational and positional errors between the two scans, using methods developed for alignment of stress/rest image pairs [61]. Subsequently, the contours derived from the rest perfusion data are applied to the spatially co-registered <sup>18</sup>F-FDG images. Quantification of the viability scores (mismatch and scar regions) is performed after direct image count normalization between the perfusion and viability scans. The method of assigning mismatch and scar scores is based on the approach taken in the PARR-1 study [59], which involves automatic registration and utilization of normal limits for resting perfusion. The viability analysis is performed in polar coordinates, with computation of scar and mismatch scores for each patient’s polar map within the spatial location of the resting perfusion defect, as defined by total perfusion deficit analysis [62]. When the normalized perfusion value at a given polar map location is lower than the normalized <sup>18</sup>F-FDG uptake, the mismatch score is calculated from the difference between the two values. The scar score is calculated relative to the normalized <sup>18</sup>F-FDG uptake in each polar map segment. When normalized perfusion exceeds <sup>18</sup>F-FDG uptake, the scar score is assigned a value equal to the normalized perfusion value in that segment. The total scar score in the entire polar map is then computed as the sum of all segmental scar and mismatch scores, and reported as a percentage of the total area of the left myocardium. An example of mismatch and scar quantification is shown in Fig. 8.

Quantitative analysis of mismatch and scar has been used in several clinical trials. The original technique

developed by the Ottawa group was utilized in the PARR-1 and PARR-2 trials [59, 63]. The objective of the PARR-1 trial by Beanlands et al. [59] was to determine whether the extent of the viability (mismatch or scar) is related to the amount of recovery of left ventricular function and to develop a model predicting recovery after revascularization, based on the viability imaging results. They found that the quantitative measure of scar was a significant independent predictor of left ventricular function recovery after revascularization. In a subsequent sub-study of the PARR-2 trial, the investigators found that in 182 patients with ischemic left ventricular dysfunction, the risk of cardiac death, myocardial infarction or cardiac-related re-hospitalization was reduced when a quantitative mismatch variable was above 7 % [63]. Quantitative analysis of mismatch and scar was also recently applied by Uebleis et al. [64] in 244 patients to evaluate the prognostic significance of <sup>18</sup>F-FDG-PET viability scanning for the prediction of patients with ischemic cardiomyopathy and left ventricular dysfunction. Their analysis showed that the patients with mismatch greater than 5 % (as established by the quantitative software) who did not undergo early revascularization had significantly higher mortality than the group who had similar mismatch (≥5 %) and did undergo the intervention. This study illustrates the role of quantitative viability imaging in the selection of patients for appropriate therapy. It would have been very difficult to derive such definite mismatch thresholds, which can be used to guide therapy, had quantitative analysis not been employed.

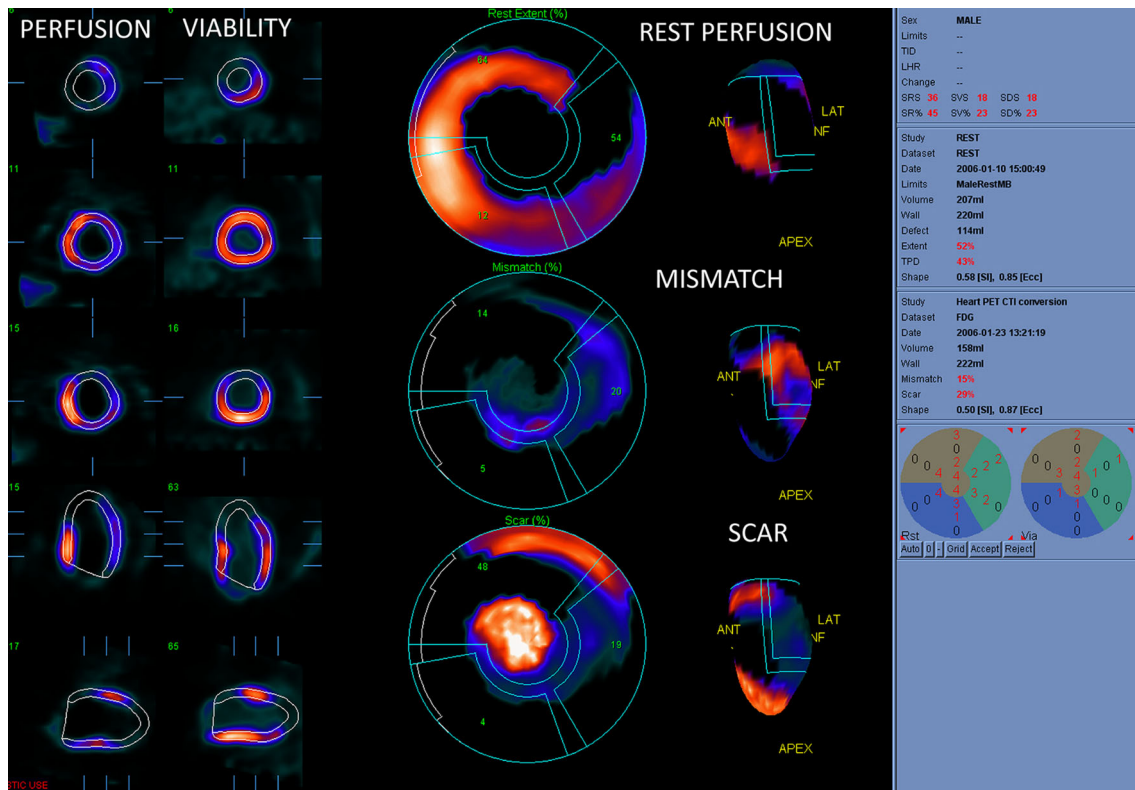


**Fig. 8** Viability quantification by PET. Rest perfusion images and viability images are shown (*two left columns*). Polar map quantification (*middle column* and 3D representation, *right column*) shows

resting perfusion defect with total perfusion deficit of 43 % (*top polar map*) Mismatch of 15 % (*middle polar map*) and scar of 29 % (*bottom polar map*) (color figure online)

### Absolute quantification of myocardial metabolism

Imbalances in cardiac metabolism are related to several cardiovascular disorders. PET techniques, by radiolabeling and measuring the kinetics of metabolic substrates, allow in vivo quantification of glucose uptake, oxygen consumption and fatty acid oxidation in the heart. The relative quantification of a radiotracer can be accomplished by static viability imaging as described earlier, but quantification of glucose metabolism in absolute units is possible only through dynamic quantitative  $^{18}\text{F}$ -FDG imaging [58, 65, 66]. Tracer kinetic compartmental models have been developed for the analysis of  $^{18}\text{F}$ -FDG metabolism and allow computation of regional glucose utilization rates in  $\mu\text{mol}/\text{min}/\text{g}$  both at stress and at rest [66]. The mismatch between blood flow and glucose utilization could be used to establish the presence of “metabolic ischemia”. Such quantitative imaging methods could perhaps play a role in the therapeutic management of patients with cardiomyopathy. The use of  $^{18}\text{F}$ -FDG for metabolic imaging and quantification is clinically feasible, since it does not require a cyclotron on site and  $^{18}\text{F}$ -FDG is a routinely available tracer.

In addition, oxidative metabolism of the myocardium can be assessed by  $^{11}\text{C}$ -palmitate [67] or  $^{11}\text{C}$ -acetate tracers [68, 69] tracers (although these tracers require a cyclotron on site). Quantitative kinetic models for  $^{11}\text{C}$ -acetate have been developed to derive, non-invasively, the regional myocardial clearance rates of  $^{11}\text{CO}_2$  (turnover rate constant in 1/min) from the myocardium [68, 69]. Based on invasive comparisons in canine studies, these values could be calibrated to absolute units ( $\mu\text{mol}/\text{min}/\text{g}$ ) reflecting the myocardial oxygen consumption.  $^{11}\text{C}$ -acetate imaging has been shown in human studies to identify hibernating myocardium potentially better than viability studies using  $^{18}\text{F}$ -FDG [70].  $^{11}\text{C}$ -palmitate tracer kinetic modeling is more complex than  $^{11}\text{C}$ -acetate modeling and it allows in vivo evaluation of the reduction of fatty acid oxidation in the ischemic myocardium [67, 71, 72]. The regional relative uptake and time-activity curves can be derived to estimate the clearance half times and the retention fraction of the  $^{11}\text{C}$ -palmitate from the myocardium [71]. This technique could potentially be used to evaluate the consequences of the ischemic injury. Nevertheless, these sophisticated quantitative techniques for evaluation of myocardial oxidative metabolism originally established and validated

primarily in animal models have, largely, not been used clinically to date.

### PET quantification and hybrid imaging

Virtually all PET scanners are offered currently by vendors in hybrid PET/CT configuration. Many of these systems feature high-end (64-slice or higher) CT components, capable of state-of-the-art CT coronary angiography (CTA). Several groups have investigated the feasibility of obtaining improved diagnostic performance by augmenting quantitative PET analysis with anatomical information from coronary CTA. Kajander et al. [73] studied the quantitative combined analysis of  $^{15}\text{O}$ -water PET blood flow and coronary CTA. They demonstrated that the combination of PET and coronary CTA achieves 95 % sensitivity and 100 % specificity, allowing higher diagnostic accuracy than either CTA or PET alone. In a similar study, Danad et al. [74] found that the diagnostic accuracy of quantitative  $^{15}\text{O}$ -water PET/CTA was superior to that of either  $^{15}\text{O}$ -water PET or CTA alone for the detection of clinically significant CAD.

Combined quantitative analysis of PET and CTA requires perfect alignment of the PET and CT scans. This cannot be guaranteed simply by ensuring that the patient does not move on the bed, since CTA and PET are typically acquired with different breathing patterns. The alignment can be performed interactively; however, such manual intervention is likely to introduce inter-observer variability into the hybrid imaging results. Nakazato et al. [75] validated a fully automated technique for the alignment of PET and CTA. They found that despite CTA and PET scans being performed without the patient leaving the table, misalignments between PET and CTA were typically between 14 and 27 mm. The automated software successfully corrected these misalignments, allowing combined 3D visualization of coronary vessel anatomy and hypoperfusion. Subsequently, the quantitative results were modified in 11 out of 32 studies based on the co-registration with CTA [75]. Such 3D fusion of the anatomical and functional scans may allow more precise left ventricular contouring and vascular territory adjustment for subsequent quantitative analysis.

### Vulnerable plaque quantification

Positron emission tomography imaging could also be utilized to characterize atherosclerotic plaque deposits within vessel walls. Elevated macrophage content and associated histological evidence of inflammation are the major hallmarks of ruptured arterial plaques. Among the tracer

compounds for imaging macrophage accumulation,  $^{18}\text{F}$ -FDG is approved for human scanning and is used extensively for the detection and staging of tumors, and for imaging of the glucose utilization in viable myocardium [76] (see previous sections).  $^{18}\text{F}$ -FDG is currently the most validated PET compound for vulnerable plaque imaging [77]. High-end PET/CT with 64-slice (or higher) CT allows precise anatomical delineation of the plaque and vessel anatomy by CTA. PET studies of plaque inflammation in the carotid vessels [78] and in the aorta [79] have been reported. Thanks to the increased PET imaging resolution of the new hybrid PET/CT scanners, it may also be possible to image coronary arteries. Increased  $^{18}\text{F}$ -FDG signal along the course of the coronary arteries in patients with known CAD has been reported, but without direct confirmation that plaques existed at the sites of increased uptake [80]. Higher  $^{18}\text{F}$ -FDG signal at culprit plaque sites was shown in patients with acute coronary syndrome [81]. Another preliminary study with 64-slice PET/CT also found increased  $^{18}\text{F}$ -FDG uptake at culprit sites of acute myocardial infarction after coronary stenting [82]. The other PET tracer that can potentially depict coronary plaque biology and is approved for human scanning is  $^{18}\text{F}$ -sodium fluoride. Preliminary hybrid PET/CT imaging in coronaries with  $^{18}\text{F}$ -sodium fluoride has been performed [83]. It has also been shown, in a longitudinal  $^{18}\text{F}$ -FDG-PET/CT study, that focal arterial inflammation precedes subsequent calcification in the same location [84].

The quantification of vascular atherosclerotic plaques from PET images presents new challenges. In cases of plaque inflammation, small hot spots need to be differentiated from uptake in other adjacent structures. In the monitoring of the disease progression, the level of focal activity may need to be compared in patients with suspected inflammation versus controls, or versus previous studies. The analysis techniques are similar to the methods used in oncological imaging for tracer uptake quantification in tumors. Typically, SUVs or target-to-background ratios are used in the analysis of the vascular plaque uptake [82, 83, 85, 86]. Small plaque sizes and the need for partial volume correction, especially in the coronary vessels, may make quantification of SUVs problematic. New PET reconstruction techniques, which employ resolution recovery principles, can aid in the correction of the tracer activity localized in small lesions [87]. The regions of interest are most robustly guided by coregistered CTA, which provides the anatomical definition of the plaque boundaries. Although it is possible to judge tracer uptake in the vasculature by visual grading, the results are highly variable. Quantification of target-to-background ratios or SUVs allows detection of subtle, but significant increases the tracer concentration in inflamed plaques. In an example from our study of coronary plaque imaging with PET, we

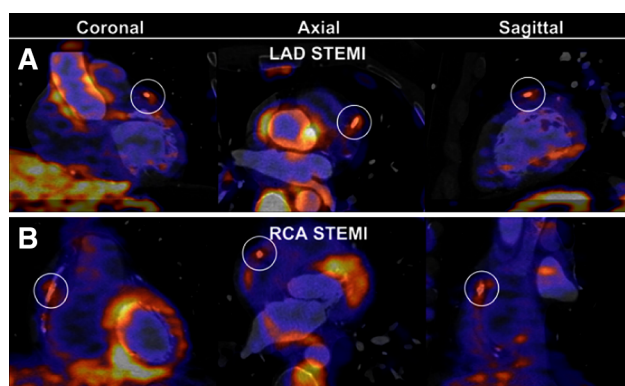


**Fig. 9** PET  $^{18}\text{F}$ -FDG coronary uptake quantification. Examples of increased  $^{18}\text{F}$ -FDG uptake at stent site in patients with acute ST elevation myocardial infarction (STEMI). **a** A 54-year-old man imaged after percutaneous coronary stenting of proximal left anterior descending artery (LAD) for STEMI. Quantification of maximum target-to background ratio (maxTBR) at stent site was 2.1 (white circles). **b** A 49-year-old man imaged after stenting of proximal right coronary artery (RCA) for STEMI. maxTBR at stent site was 2.1. Reproduced with permission from Cheng et al. [82] (color figure online)

show the quantification of  $^{18}\text{F}$ -FDG atherosclerotic plaque uptake in two cases with acute coronary syndrome (Fig. 9).

### Future directions

As hybrid PET/CT scanners become more ubiquitous and image analysis becomes more automated, we will likely see some integration of the quantitative CT and or CTA results with PET results, since visual hybrid analysis of the data from these two modalities has been shown to have incremental diagnostic value [73]. Additionally, a calcium scoring scan, which can be readily obtained on any PET/CT scanner, could perhaps be used in conjunction with the PET images for enhanced diagnosis or prognosis. For example, Bybee et al. [88] studied patients with no history of prior CAD and normal PET perfusion scans and found a high prevalence of significant subclinical atherosclerosis in patients who had elevated calcium scores. Thus, it is possible that quantitative combination of multiple parameters obtained from both CT or CTA and multiple PET parameters could be developed to derive integrated quantitative scores expressing the risk of disease, as has been demonstrated for SPECT imaging [89].

Concerns about radiation dose will influence the use of hybrid PET/CT or PET/CTA scanning. In efforts to reduce the dose and scan time, software methods have been proposed for PET attenuation correction using CT calcium scoring scans [90], eliminating the need for CT attenuation map scans. On the other hand, it is also potentially possible to obtain calcium scores from the attenuation maps [91]

and use them as an additional independent marker of the disease. Low-dose protocols have been proposed for hybrid PET/CTA imaging [92]. It has been reported that hyperemic (stress) blood flow alone (without rest scan) may be sufficient for detection of obstructive CAD [74]. Therefore, combining physiological and anatomical imaging could be accomplished with PET stress-only/CTA imaging, which could significantly reduce the overall dose burden and scan duration [92, 93]. Furthermore, prospective gating and other dose-reducing techniques allow acquisition of high quality coronary CTA scans with doses lower than 1 mSv [94]. These novel CT acquisition techniques may facilitate more routine use of hybrid PET/CTA imaging and hybrid quantification. Finally, cardiac PET/MR has entered the clinical arena allowing further reduction of the overall radiation dose and may also offer some new clinical applications such as imaging of cardiac sarcoidosis [95].

It is also likely that cardiac respiratory gating [96, 97] and advanced PET reconstruction techniques, available with the new equipment, will increase resolution and allow better definition of motion for PET images. Further, it may allow improvement of the accuracy of the quantification methods by the analysis of the motion-frozen data [98]. Consequently, very high quality, high-resolution PET images free of patient and respiratory and cardiac motion could perhaps enable quantification of endocardial and epicardial perfusion and absolute myocardial blood flow. Such high-resolution quantification will, very likely, also be required for vulnerable plaque quantification in the coronary arteries to avoid partial volume and motion effects.

### Summary

Positron emission tomography cardiovascular imaging is a powerful clinical and research tool. It allows determination of the extent and severity of CAD, identification of early coronary disease by absolute myocardial flow measurements, detection of viable myocardium, determination of myocardial metabolism, measurement of cardiac function, and potential differentiation of vulnerable plaques from stable plaques. Additional synergistic possibilities exist when it is coupled with CTA. A multitude of clinically relevant cardiovascular imaging parameters can be obtained from PET imaging. Some of these variables are inherently quantitative and it is not possible to use visual analysis for their determination (such as absolute myocardial blood flow obtained from dynamic data, phase analysis or ejection fraction and systolic/diastolic volumes obtained from gated data). Other variables such as relative myocardial hypoperfusion, myocardial viability or tracer plaque uptake have traditionally been assessed by visual means,

but quantitative methods allow improved reproducibility and potentially also improved accuracy. The quantification of PET images allows objective determination of the disease likelihood and appropriate risk stratification. Virtually all quantitative functional and perfusion parameters can be obtained rapidly (typically in a matter of seconds) from reconstructed tomographic data with minimal user interaction. For these reasons, the use of advanced objective quantification methods in cardiovascular PET is becoming an integral part of clinical examinations and represents a primary advantage over other modalities.

**Conflict of interest** Cedars-Sinai Medical Center receives royalties for the quantitative assessment of function, perfusion, and viability, a portion of which is distributed to the authors of this manuscript (DB, GG, PS).

**Human and Animal Studies** This article does not contain any studies with human or animal subjects performed by any of the authors.

## References

- Naya M, Murthy VL, Taqueti VR et al (2014) Preserved coronary flow reserve effectively excludes high-risk coronary artery disease on angiography. *J Nucl Med* 55:248–255
- Murthy VL, Naya M, Foster CR et al (2011) Improved cardiac risk assessment with noninvasive measures of coronary flow reserve. *Circulation* 124:2215–2224
- Camici PG, Rimoldi OE (2009) The clinical value of myocardial blood flow measurement. *J Nucl Med* 50(7):1076–1087
- Gould KL, Johnson NP, Bateman TM et al (2013) Anatomic versus physiologic assessment of coronary artery disease. Role of coronary flow reserve, fractional flow reserve, and positron emission tomography imaging in revascularization decision-making. *J Am Coll Cardiol* 62:1639–1653
- Wijns W, Vatner SF, Camici PG (1998) Hibernating myocardium. *N Engl J Med* 339:173–181
- Joshi F, Rosenbaum D, Bordes S, Rudd JH (2011) Vascular imaging with positron emission tomography. *J Intern Med* 270:99–109
- Klocke FJ, Baird MG, Lorell BH et al (2003) ACC/AHA/ASNC guidelines for the clinical use of cardiac radionuclide imaging—executive summary: a report of the American College of Cardiology/American Heart Association Task Force on Practice Guidelines (ACC/AHA/ASNC Committee to Revise the 1995 Guidelines for the Clinical Use of Cardiac Radionuclide Imaging). *Circulation* 108:1404–1418
- Sampson UK, Dorbala S, Limaye A, Kwong R, Di Carli MF (2007) Diagnostic accuracy of rubidium-82 myocardial perfusion imaging with hybrid positron emission tomography/computed tomography in the detection of coronary artery disease. *J Am Coll Cardiol* 49:1052–1058
- Santana CA, Folks RD, Garcia EV et al (2007) Quantitative (<sup>82</sup>Rb) PET/CT: development and validation of myocardial perfusion database. *J Nucl Med* 48:1122–1128
- Nakazato R, Berman DS, Dey D et al (2012) Automated quantitative Rb-82 3D PET/CT myocardial perfusion imaging: normal limits and correlation with invasive coronary angiography. *J Nucl Cardiol* 19:265–276
- Arsanjani R, Xu Y, Hayes SW et al (2013) Comparison of fully automated computer analysis and visual scoring for detection of coronary artery disease from myocardial perfusion SPECT in a large population. *J Nucl Med* 54:221–228
- Xu Y, Hayes S, Ali I et al (2010) Automatic and visual reproducibility of perfusion and function measures for myocardial perfusion SPECT. *J Nucl Cardiol* 17:1050–1057
- Beanlands RS, Chow BJ, Dick A et al (2007) CCS/CAR/CANM/CNCS/CanSCMR joint position statement on advanced noninvasive cardiac imaging using positron emission tomography, magnetic resonance imaging and multidetector computed tomographic angiography in the diagnosis and evaluation of ischemic heart disease—executive summary. *Can J Cardiol* 23:107–119
- Marzilli M, Merz CN, Boden WE et al (2012) Obstructive coronary atherosclerosis and ischemic heart disease: an elusive link! *J Am Coll Cardiol* 60:951–956
- Kaster T, Mylonas I, Renaud JM, Wells GA, Beanlands RSB, deKemp RA (2012) Accuracy of low-dose rubidium-82 myocardial perfusion imaging for detection of coronary artery disease using 3D PET and normal database interpretation. *J Nucl Cardiol* 19:1135–1145
- Klingensmith WC 3rd, Noonan C, Goldberg JH, Buchwald D, Kimball JT, Manson SM (2009) Decreased perfusion in the lateral wall of the left ventricle in PET/CT studies with <sup>13</sup>N-ammonia: evaluation in healthy adults. *J Nucl Med Technol* 37:215–219
- Germano G, Kavanagh PB, Slomka PJ, Van Kriekinge SD, Pollard G, Berman DS (2007) Quantitation in gated perfusion SPECT imaging: the Cedars-Sinai approach. *J Nucl Cardiol* 14:433–454
- Schaefer WM, Lipke CS, Nowak B et al (2003) Validation of an evaluation routine for left ventricular volumes, ejection fraction and wall motion from gated cardiac FDG PET: a comparison with cardiac magnetic resonance imaging. *Eur J Nucl Med Mol Imaging* 30:545–553
- Li Y, Wang L, Zhao SH et al (2014) Gated F-18 FDG PET for assessment of left ventricular volumes and ejection fraction using QGS and 4D-MSPECT in patients with heart failure: a comparison with cardiac MRI. *PLoS ONE* 9:e80227
- Wang L, Zhang Y, Yan C et al (2013) Evaluation of right ventricular volume and ejection fraction by gated (<sup>18</sup>F)-FDG PET in patients with pulmonary hypertension: comparison with cardiac MRI and CT. *J Nucl Cardiol* 20:242–252
- Lertsburapa K, Ahlberg AW, Bateman TM et al (2008) Independent and incremental prognostic value of left ventricular ejection fraction determined by stress gated rubidium 82 PET imaging in patients with known or suspected coronary artery disease. *J Nucl Cardiol* 15:745–753
- Pazhenkottil AP, Buechel RR, Nkoulou R et al (2011) Left ventricular dyssynchrony assessment by phase analysis from gated PET-FDG scans. *J Nucl Cardiol* 18:920–925
- AlJaroudi W, Alraies MC, Hachamovitch R et al (2012) Association of left ventricular mechanical dyssynchrony with survival benefit from revascularization: a study of gated positron emission tomography in patients with ischemic LV dysfunction and narrow QRS. *Eur J Nucl Med Mol Imaging* 39:1581–1591
- Lehner S, Uebles C, Schussler F et al (2013) The amount of viable and dyssynchronous myocardium is associated with response to cardiac resynchronization therapy: initial clinical results using multiparametric ECG-gated [<sup>18</sup>F]FDG PET. *Eur J Nucl Med Mol Imaging* 40:1876–1883
- Xu Y, Arsanjani R, Clond M et al (2012) Transient ischemic dilation for coronary artery disease in quantitative analysis of same-day sestamibi myocardial perfusion SPECT. *J Nucl Cardiol* 19:465–473
- Rischpler C, Higuchi T, Fukushima K et al (2012) Transient ischemic dilation ratio in <sup>82</sup>Rb PET myocardial perfusion

- imaging: normal values and significance as a diagnostic and prognostic marker. *J Nucl Med* 53:723–730
27. Dorbala S, Vangala D, Sampson U, Limaye A, Kwong R, Di Carli MF (2007) Value of vasodilator left ventricular ejection fraction reserve in evaluating the magnitude of myocardium at risk and the extent of angiographic coronary artery disease: a  $^{82}\text{Rb}$  PET/CT study. *J Nucl Med* 48:349–358
  28. Dorbala S, Hachamovitch R, Curillova Z et al (2009) Incremental prognostic value of gated Rb-82 positron emission tomography myocardial perfusion imaging over clinical variables and rest LVEF. *JACC Cardiovasc Imaging* 2:846–854
  29. Hsiao E, Ali B, Blankstein R et al (2013) Detection of obstructive coronary artery disease using regadenoson stress and  $^{82}\text{Rb}$  PET/CT myocardial perfusion imaging. *J Nucl Med* 54:1748–1754
  30. Choi Y, Huang SC, Hawkins RA, Kuhle WG, Dahlbom M, Hoh CK, Czernin J, Phelps ME, Schelbert HR (1993) A simplified method for quantification of myocardial blood flow using nitrogen-14 ammonia and dynamic PET. *J Nucl Med* 34:488–497
  31. Choi Y, Huang SC, Hawkins RA, Kim JY, Kim BT, Hoh CK, Chen K, Phelps ME, Schelbert HR (1999) Quantification of myocardial blood flow using N-13-ammonia and PET: comparison of tracer models. *J Nucl Med* 40:1045–1055
  32. Katoh C, Morita K, Shiga T, Kubo N, Nakada K, Tamaki N (2004) Improvement of algorithm for quantification of regional myocardial blood flow using  $^{15}\text{O}$ -water with PET. *J Nucl Med* 45:1908–1916
  33. Lortie M, Beanlands RS, Yoshinaga K, Klein R, Dasilva JN, DeKemp RA (2007) Quantification of myocardial blood flow with  $^{82}\text{Rb}$  dynamic PET imaging. *Eur J Nucl Med* 34:1765–1774
  34. El Fakhri G, Kardan A, Sitek A et al (2009) Reproducibility and accuracy of quantitative myocardial blood flow assessment with ( $^{82}\text{Rb}$ ) PET: comparison with ( $^{13}\text{N}$ -ammonia) PET. *J Nucl Med* 50:1062–1071
  35. deKemp RA, Declerck J, Klein R et al (2013) Multisoftware reproducibility study of stress and rest myocardial blood flow assessed with 3D dynamic PET/CT and a 1-tissue-compartment model of  $^{82}\text{Rb}$  kinetics. *J Nucl Med* 54:571–577
  36. Slomka PJ, Alexanderson E, Jacome R et al (2012) Comparison of clinical tools for measurements of regional stress and rest myocardial blood flow assessed with  $^{13}\text{N}$ -ammonia PET/CT. *J Nucl Med* 53:171–181
  37. Prior JO, Allenbach G, Valenta I et al (2012) Quantification of myocardial blood flow with  $^{82}\text{Rb}$  positron emission tomography: clinical validation with  $^{15}\text{O}$ -water. *Eur J Nucl Med Mol Imaging* 39:1037–1047
  38. Schelbert HR (2010) Anatomy and physiology of coronary blood flow. *J Nucl Cardiol* 17:545–554
  39. Johnson NP, Gould KL (2005) Clinical evaluation of a new concept: resting myocardial perfusion heterogeneity quantified by markovian analysis of PET identifies coronary microvascular dysfunction and early atherosclerosis in 1,034 subjects. *J Nucl Med* 46:1427–1437
  40. Kaufmann PA, Rimoldi OE, Gnecci-Ruscone T, Luscher TF, Camici PG (2007) Systemic nitric oxide synthase inhibition improves coronary flow reserve to adenosine in patients with significant stenoses. *Am J Physiol Heart Circ Physiol* 293:H2178–H2182
  41. Van Tosh A, Votaw JR, Reichek N, Palestro CJ, Nichols KJ (2013) The relationship between ischemia-induced left ventricular dysfunction, coronary flow reserve, and coronary steal on regadenoson stress-gated ( $^{82}\text{Rb}$ ) PET myocardial perfusion imaging. *J Nucl Cardiol* 20:1060–1068
  42. Heijne M, Raijmakers PG, Harms HJ et al (2010) Coronary steal: revealing the diagnosis with quantitative cardiac PET/CT. *J Nucl Cardiol* 17:1118–1121
  43. Baller D, Notohamiprodjo G, Gleichmann U, Holzinger J, Weise R, Lehmann J (1999) Improvement in coronary flow reserve determined by positron emission tomography after 6 months of cholesterol-lowering therapy in patients with early stages of coronary atherosclerosis. *Circulation* 99:2871–2875
  44. Parkash R, deKemp RA, Ruddy TD et al (2004) Potential utility of rubidium 82 PET quantification in patients with 3-vessel coronary artery disease. *J Nucl Cardiol* 11:440–449
  45. Ziadi MC, Dekemp RA, Williams K et al (2012) Does quantification of myocardial flow reserve using rubidium-82 positron emission tomography facilitate detection of multivessel coronary artery disease? *J Nucl Cardiol* 19:670–680
  46. Fiechter M, Ghadri JR, Gebhard C et al (2012) Diagnostic value of  $^{13}\text{N}$ -ammonia myocardial perfusion PET: added value of myocardial flow reserve. *J Nucl Med* 53:1230–1234
  47. Maddahi J (2012) Properties of an ideal PET perfusion tracer: new PET tracer cases and data. *J Nucl Cardiol* 19(Suppl 1):S30–S37
  48. Berman DS, Maddahi J, Tamarappoo BK et al (2013) Phase II safety and clinical comparison with single-photon emission computed tomography myocardial perfusion imaging for detection of coronary artery disease: flurpiridaz F 18 positron emission tomography. *J Am Coll Cardiol* 61:469–477
  49. Sherif HM, Nekolla SG, Saraste A et al (2011) Simplified quantification of myocardial flow reserve with flurpiridaz F 18: validation with microspheres in a pig model. *J Nucl Med* 52:617–624
  50. Berman DS, Germano G, Slomka PJ (2012) Improvement in PET myocardial perfusion image quality and quantification with flurpiridaz F 18. *J Nucl Cardiol* 19(Suppl 1):S38–S45
  51. Woo J, Tamarappoo B, Dey D et al (2011) Automatic 3D registration of dynamic stress and rest ( $^{82}\text{Rb}$ ) and flurpiridaz F 18 myocardial perfusion PET data for patient motion detection and correction. *Med Phys* 38:6313–6326
  52. Schinkel AF, Bax JJ, Poldermans D, Elhendy A, Ferrari R, Rahimtoola SH (2007) Hibernating myocardium: diagnosis and patient outcomes. *Curr Probl Cardiol* 32:375–410
  53. Klein C, Nekolla SG, Bengel FM et al (2002) Assessment of myocardial viability with contrast-enhanced magnetic resonance imaging: comparison with positron emission tomography. *Circulation* 105:162–167
  54. Slart RH, Bax JJ, van Veldhuisen DJ et al (2006) Prediction of functional recovery after revascularization in patients with coronary artery disease and left ventricular dysfunction by gated FDG-PET. *J Nucl Cardiol* 13:210–219
  55. Desideri A, Cortigiani L, Christen AI et al (2005) The extent of perfusion-F18-fluorodeoxyglucose positron emission tomography mismatch determines mortality in medically treated patients with chronic ischemic left ventricular dysfunction. *J Am Coll Cardiol* 46:1264–1269
  56. Zhang X, Liu XJ, Hu S et al (2008) Long-term survival of patients with viable and nonviable aneurysms assessed by  $^{99\text{m}}\text{Tc}$ -MIBI SPECT and  $^{18}\text{F}$ -FDG PET: a comparative study of medical and surgical treatment. *J Nucl Med* 49:1288–1298
  57. Santana CA, Faber TL, Soler-Peter M et al (2008) Prognostic performance of quantitative PET tools for stratification of patients with ischemic cardiomyopathy undergoing myocardial viability assessment. *Nucl Med Commun* 29:970–981
  58. Anagnostopoulos C, Georgakopoulos A, Pianou N, Nekolla SG (2013) Assessment of myocardial perfusion and viability by positron emission tomography. *Int J Cardiol* 167:1737–1749
  59. Beanlands RSB, Ruddy TD, deKemp RA et al (2002) Positron emission tomography and recovery following revascularization (PARR-1): the importance of scar and the development of a prediction rule for the degree of recovery of left ventricular function. *J Am Coll Cardiol* 40:1735–1743

60. Ling LF, Marwick TH, Flores DR et al (2013) Identification of therapeutic benefit from revascularization in patients with left ventricular systolic dysfunction: inducible ischemia versus hibernating myocardium. *Circ Cardiovasc Imaging* 6:363–372
61. Slomka PJ, Nishina H, Berman DS et al (2004) Automatic quantification of myocardial perfusion stress-rest change: a new measure of ischemia. *J Nucl Med* 45:183–191
62. Slomka PJ, Nishina H, Berman DS et al (2005) Automated quantification of myocardial perfusion SPECT using simplified normal limits. *J Nucl Cardiol* 12:66–77
63. D'Egidio G, Nichol G, Williams KA et al (2009) Increasing benefit from revascularization is associated with increasing amounts of myocardial hibernation: a substudy of the PARR-2 trial. *JACC Cardiovasc Imaging* 2:1060–1068
64. Uebleis C, Hellweger S, Laubender RP et al (2013) The amount of dysfunctional but viable myocardium predicts long-term survival in patients with ischemic cardiomyopathy and left ventricular dysfunction. *Int J Cardiovasc Imaging* 29:1645–1653
65. Marshall RC, Huang SC, Nash WW, Phelps ME (1983) Assessment of the [<sup>18</sup>F]fluorodeoxyglucose kinetic model in calculations of myocardial glucose metabolism during ischemia. *J Nucl Med* 24:1060–1064
66. Nienaber CA, Gambhir SS, Mody FV et al (1993) Regional myocardial blood flow and glucose utilization in symptomatic patients with hypertrophic cardiomyopathy. *Circulation* 87:1580–1590
67. Schon HR, Schelbert HR, Najafi A et al (1982) C- 11 labeled palmitic acid for the noninvasive evaluation of regional myocardial fatty acid metabolism with positron-computed tomography. II. Kinetics of C-11 palmitic acid in acutely ischemic myocardium. *Am Heart J* 103:548–561
68. Brown MA, Myears DW, Bergmann SR (1988) Noninvasive assessment of canine myocardial oxidative metabolism with carbon-11 acetate and positron emission tomography. *J Am Coll Cardiol* 12:1054–1063
69. Walsh MN, Geltman EM, Brown MA et al (1989) Noninvasive estimation of regional myocardial oxygen consumption by positron emission tomography with carbon-11 acetate in patients with myocardial infarction. *J Nucl Med* 30:1798–1808
70. Gropler RJ, Geltman EM, Sampathkumaran K et al (1993) Comparison of carbon-11-acetate with fluorine-18-fluorodeoxyglucose for delineating viable myocardium by positron emission tomography. *J Am Coll Cardiol* 22:1587–1597
71. Schwaiger M, Schelbert HR, Keen R et al (1985) Retention and clearance of C-11 palmitic acid in ischemic and reperfused canine myocardium. *J Am Coll Cardiol* 6:311–320
72. Schwaiger M, Schelbert HR, Ellison D et al (1985) Sustained regional abnormalities in cardiac metabolism after transient ischemia in the chronic dog model. *J Am Coll Cardiol* 6:336–347
73. Kajander SA, Joutsiniemi E, Saraste M et al (2011) Clinical value of absolute quantification of myocardial perfusion with (<sup>15</sup>O)-water in coronary artery disease. *Circ Cardiovasc Imaging* 4:678–684
74. Danad I, Raijmakers PG, Appelman YE et al (2013) Hybrid imaging using quantitative H215O PET and CT-based coronary angiography for the detection of coronary artery disease. *J Nucl Med* 54:55–63
75. Nakazato R, Dey D, Alexanderson E et al (2012) Automatic alignment of myocardial perfusion PET and 64-slice coronary CT angiography on hybrid PET/CT. *J Nucl Cardiol* 19:482–491
76. Maddahi J, Schelbert H, Brunken R, Di Carli M (1994) Role of thallium-201 and PET imaging in evaluation of myocardial viability and management of patients with coronary artery disease and left ventricular dysfunction. *J Nucl Med* 35:707–715
77. Vancaerneyest D, Pasquet A, Roelants V, Gerber BL, Vanoverschelde JL (2011) Imaging the vulnerable plaque. *J Am Coll Cardiol* 57:1961–1979
78. Rudd JH, Warburton EA, Fryer TD et al (2002) Imaging atherosclerotic plaque inflammation with [<sup>18</sup>F]-fluorodeoxyglucose positron emission tomography. *Circulation* 105:2708–2711
79. Tatsumi M, Cohade C, Nakamoto Y, Wahl RL (2003) Fluorodeoxyglucose uptake in the aortic wall at PET/CT: possible finding for active atherosclerosis. *Radiology* 229:831–837
80. Wykrzykowska J, Lehman S, Williams G et al (2009) Imaging of inflamed and vulnerable plaque in coronary arteries with <sup>18</sup>F-FDG PET/CT in patients with suppression of myocardial uptake using a low-carbohydrate, high-fat preparation. *J Nucl Med* 50:563–568
81. Rogers IS, Nasir K, Figueroa AL et al (2010) Feasibility of FDG imaging of the coronary arteries: comparison between acute coronary syndrome and stable angina. *JACC Cardiovasc Imaging* 3:388–397
82. Cheng VY, Slomka PJ, Le Meunier L et al (2012) Coronary arterial <sup>18</sup>F-FDG uptake by fusion of PET and coronary CT angiography at sites of percutaneous stenting for acute myocardial infarction and stable coronary artery disease. *J Nucl Med* 53:575–583
83. Dweck MR, Chow MW, Joshi NV et al (2012) Coronary arterial <sup>18</sup>F-sodium fluoride uptake: a novel marker of plaque biology. *J Am Coll Cardiol* 59:1539–1548
84. Abdelbaky A, Corsini E, Figueroa AL et al (2013) Focal arterial inflammation precedes subsequent calcification in the same location: a longitudinal FDG-PET/CT study. *Circ Cardiovasc Imaging* 6:747–754
85. Rogers IS, Tawakol A (2011) Imaging of coronary inflammation with FDG-PET: feasibility and clinical hurdles. *Curr Cardiol Rep* 13:138–144
86. Joshi NV, Vesey AT, Williams MC et al (2014) <sup>18</sup>F-fluoride positron emission tomography for identification of ruptured and high-risk coronary atherosclerotic plaques: a prospective clinical trial. *Lancet* 383:705–713
87. Panin VY, Kehren F, Michel C, Casey M (2006) Fully 3-D PET reconstruction with system matrix derived from point source measurements. *IEEE Trans Med Imaging* 25:907–921
88. Bybee KA, Lee J, Markiewicz R et al (2010) Diagnostic and clinical benefit of combined coronary calcium and perfusion assessment in patients undergoing PET/CT myocardial perfusion stress imaging. *J Nucl Cardiol* 17:188–196
89. Arsanjani R, Xu Y, Dey D et al (2013) Improved accuracy of myocardial perfusion SPECT for detection of coronary artery disease by machine learning in a large population. *J Nucl Cardiol* 20:553–562
90. Zaidi H, Nkoulou R, Bond S et al (2013) Computed tomography calcium score scan for attenuation correction of N-13 ammonia cardiac positron emission tomography: effect of respiratory phase and registration method. *Int J Cardiovasc Imaging* 29:1351–1360
91. Mylonas I, Kazmi M, Fuller L et al (2012) Measuring coronary artery calcification using positron emission tomography-computed tomography attenuation correction images. *Eur Heart J Cardiovasc Imaging* 13:786–792
92. Kajander S, Ukkonen H, Sipilä H, Teräs M, Knuuti J (2009) Low radiation dose imaging of myocardial perfusion and coronary angiography with a hybrid PET/CT scanner. *Clin Physiol Funct Imaging* 29:81–88
93. Kajander S, Joutsiniemi E, Saraste M et al (2010) Cardiac positron emission tomography/computed tomography imaging accurately detects anatomically and functionally significant coronary artery disease. *Circulation* 122:603–613
94. Achenbach S, Goroll T, Seltmann M et al (2011) Detection of coronary artery stenoses by low-dose, prospectively ECG-triggered, high-pitch spiral coronary CT angiography. *JACC Cardiovasc Imaging* 4:328–337
95. White JA, Rajchl M, Butler J, Thompson RT, Prato FS, Wisenberg G (2013) Active cardiac sarcoidosis: first clinical experience of

- simultaneous positron emission tomography–magnetic resonance imaging for the diagnosis of cardiac disease. *Circulation* 127:e639–e641
96. Martinez-Möller A, Zikic D, Botnar RM et al (2007) Dual cardiac–respiratory gated PET: implementation and results from a feasibility study. *Eur J Nucl Med Mol Imaging* 34:1447–1454
97. Büther F, Dawood M, Stegger L et al (2009) List mode-driven cardiac and respiratory gating in PET. *J Nucl Med* 50:674–681
98. Slomka PJ, Nishina H, Berman DS et al (2004) “Motion-frozen” display and quantification of myocardial perfusion. *J Nucl Med* 45:1128–1134